Eur. Phys. J. C (2024) 84:686
https://doi.org/10.1140/epjc/s10052-024-13057-1

THE EUROPEAN PHYSICAL JOURNAL C

Regular Article - Theoretical Physics

Testing strong gravitational lensing effects of various supermassive compact objects for the static and spherically symmetric hairy black hole by gravitational decoupling

G. Mustafa[1,a], **S. K. Maurya**[2,b]

[1] Department of Physics, Zhejiang Normal University, Jinhua 321004, People's Republic of China
[2] Department of Mathematical and Physical Sciences, College of Arts and Sciences, University of Nizwa, 616 Nizwa, Sultanate of Oman

Received: 22 March 2024 / Accepted: 18 June 2024

Abstract We investigate the strong gravitational lensing effects of various supermassive compact objects for the static and spherically symmetric hairy black hole by gravitational decoupling. To do this purpose, we first numerically calculate the strong deflection limit coefficients and strong deflection angle with the decoupling modified black hole parameter α and β. It is observed that for the lowest value of the parameter α, the strong deflection angle α_D reaches its maximum value with the parameter β and for the lowest value of the parameter β, strong deflection angle α_D reaches its minimum value with the parameter α; and also the strong deflection angle for α_D for the decoupling modified black hole is smaller than standard Schwarzschild black hole ($\alpha = 0$). We investigate the various astrophysical consequences via strong gravitational lensing by considering the example of various supermassive BHs in the centre nearby galaxies and observe that the decoupling modified black hole could be quantitatively distinguished from the standard Schwarzschild black hole ($\alpha = 0$). Findings in our observation suggest that the observational test for a decoupling-modified black hole is indeed feasible.

1 Introduction

The study of black hole (BH) spacetimes represents a crucial area of investigation within the realm of general relativity and other gravitational theories [1–4]. BHs offer a unique window into our understanding of gravitation, thermodynamics, and quantum effects in curved spacetime. Recent years have witnessed significant progress in both theoretical and observational explorations of BHs. Notably, the LIGO and Virgo collaborations detected gravitational wave signals arising from the merger of binary BHs [5–11]. Furthermore, there have been groundbreaking observations of high-resolution images of BHs at the center of our Milky Way galaxy, known as Sagittarius A* (Sgr A*), which has indeed been a significant focus of study and observation by the Event Horizon Telescope (EHT). The EHT captures high-resolution images of BHs. They also released the first-ever image of a BH, which is the supermassive BH in the center of the M87 galaxy [12].

The minimal geometric deformation was established in [13,14] to examine the outer configuration of a spherically symmetric line element with a fluid source that is ideal in the background of Randall gravity. The gravitational decoupling method aims to maintain spherical symmetry while simplifying matter configurations. Later, many researchers [15–19] used this method to develop and evaluate physically reliable solutions of compact objects. The decoupling approach has been investigated as a unique strategy for expanding the distorted solutions of the GR related to the most fundamental gravitational source in Refs. [20,21]. This strategy has led to the finding of exact and physically viable solutions for internal star configurations. The decoupling approach has been examined for cosmic applications in GR [22]. Numerous studies have been reported on compact objects in the background of decoupling approach [23–29]. In [30] authors developed a new technique to convert non-spinning BH metrics into rotating ones, while calculated unique hairy BH solution.

Gravitational lensing, a result of Einstein's general relativity, is a fundamental and prominent concept in astronomy, providing a reliable approach to investigating the strong-field nature of gravity. This phenomenon is a powerful instrument for magnifying and studying distant celestial objects, allow-

[a] e-mail: gmustafa3828@gmail.com
[b] e-mail: sunil@unizwa.edu.om (corresponding author)

Published online: 11 July 2024

ing astronomers to make more detailed views of galaxies and quasars, as well as identify elusive substances like dark matter, dark energy, and gravitational waves. It also contributes to a comprehensive understanding of numerous astronomical phenomena [31,32]. The distortion of the image of BHs with a gridding accretion fragment is a result of the strong gravitational lensing effect. During that era, astronomers measured the deflection angle caused by the sun during a solar eclipse [33]. However, such observations were realistically only feasible with the sun. The foundational work by [34] played a crucial role in establishing the groundwork for a precise lens equation. Subsequent numerical investigations, as discussed in [35,36], focused on the lensing phenomenon induced by static, spherically symmetric naked singularities. These studies provided a comprehensive examination of various lensing observables. Building on these contributions, later in [37] explored gravitational lensing within spherically symmetric and static spacetime. Numerous methods [38–49] encompassing weak and strong field limits have been put forth to study gravitational lensing around BHs. When the gravitational field is strong enough to cause substantial gravitational lensing, light approaches the source closely, resulting in large bending angles. As a result, light can travel along a variety of routes before reaching the observer, which could produce a number of pictures, arcs, and rings of the source. Besides the above methods and interesting work has been done by Ghosh and his coauthors [50–59] on deflection angle and other astrophysical relevant aspects of BH solutions.

Avestruz and his coauthors [60] presented a strong lensing identification approach that utilizes a feature extraction method from computer vision. Zitrin and Tom [61] calculated a light-traces-mass strong-lensing model of the massive lensing cluster MACS J2135.2-0102 ($z = 0.33$; hereafter MACS2135), known in part for hosting the cosmic eye galaxy lens. The weak deflection angle and shadow phenomena discussed by Ali and his collaborators [62–64] for different black hole solutions in the background of different theories of gravity. Recently, Niyaz and Ujjal [65–68] calculated the strong lensing of interesting newly developed solutions of BHs. In these conditions, phenomena including relativistic pictures, photon rings, and shadows could appear [69,70]

The organization of this paper is as follows: Sect. 2 presents a quick summary of the structure of BH spacetime using the decoupling approach. In Sect. 3, we discuss how BHs cause gravitational lensing, including the lens equation, deflection angle, and strong lensing coefficients. This section focuses on two supermassive BHs, $M87^*$ and $SgrA^*$, in the framework of decoupled BHs. The Einstein ring is also discussed in the same Sect. 3. Section 5 summarizes significant findings and draws study conclusions.

2 New BH solution via gravitational decoupling approach

This section deals with the newly calculated BH solution by Avalos and his coauthors [71] by using the Einstein field equations with the gravitational decoupling framework:

$$G_{\epsilon\varepsilon} \equiv R_{\epsilon\varepsilon} - \frac{1}{2}Rg_{\epsilon\varepsilon} = \mathcal{K}^2\tilde{T}_{\epsilon\varepsilon}, \tag{1}$$

where $\mathcal{K}^2 = \frac{8\pi G}{c^4}$ and $\tilde{T}_{\epsilon\varepsilon}$ describes the total amount of energy-momentum tensor, which is contributed by two different matter sectors as

$$\tilde{T}_{\epsilon\varepsilon} = T_{\epsilon\varepsilon} + \Theta_{\epsilon\varepsilon}. \tag{2}$$

In the above-mentioned Eq. (2), $T_{\epsilon\varepsilon}$ corresponds to a usual energy-momentum tensor, while $\Theta_{\epsilon\varepsilon}$ provides the gravitational sector of matter distribution. It is important to mention that the usual energy-momentum tensor satisfies the Bianchi identity, which leads us to the following covariantly conserved:

$$\nabla_\epsilon \tilde{T}^{\epsilon\varepsilon} = 0. \tag{3}$$

Now, by considering a static system under the effect of spherically symmetric property, which is given as

$$ds^2 = e^{\varepsilon(r)}dt^2 - e^{\epsilon(r)}dr^2 - r^2d\Omega^2, \tag{4}$$

where both the gravitational functions, i.e., $\varepsilon = \varepsilon(r)$ and $\epsilon = \epsilon(r)$ dependent on the radial coordinate r, and $d\Omega^2 = d\Theta^2 + \sin^2\Theta d\phi^2$. The Einstein field equations under the effect of the decoupling framework are calculated as follows:

$$\frac{1}{\mathcal{K}^2}\left[\frac{1}{r^2} - e^{-\epsilon}\left(\frac{1}{r^2} - \frac{\epsilon'}{r}\right)\right] = T_0^0 + \Theta_0^0, \tag{5}$$

$$\frac{1}{\mathcal{K}^2}\left[\frac{1}{r^2} - e^{-\epsilon}\left(\frac{1}{r^2} + \frac{\varepsilon'}{r}\right)\right] = T_1^1 + \Theta_1^1, \tag{6}$$

$$-\frac{e^{-\epsilon}}{4\mathcal{K}^2}\left[2\varepsilon'' + \varepsilon'^2 - \epsilon'\varepsilon' + \frac{2\varepsilon' - 2\epsilon'}{r}\right] = T_2^2 + \Theta_2^2. \tag{7}$$

Now, we are introducing the concept of an effective matter sector by using the following relations

$$\rho = T_0^0 + \Theta_0^0, \tag{8}$$

$$p_r = -T_1^1 - \Theta_1^1, \tag{9}$$

$$p_t = -T_2^2 - \Theta_2^2. \tag{10}$$

One can consider a suitable realistic solution for Eq. (1) by using the seed source through $T_{\epsilon\varepsilon}$, on neglecting the contribution of $\Theta_{\epsilon\varepsilon}$. Now, We can rewrite the revised metric form as follows:

$$ds^2 = e^{\xi(r)}dt^2 - e^{\lambda(r)}dr^2 - r^2d\Omega^2, \tag{11}$$

where

$$e^{-\lambda(r)} \equiv 1 - \frac{\mathcal{K}^2}{r}\int_0^r x^2T_0^0(x)dx = 1 - \frac{2m(r)}{r}. \tag{12}$$

In the above relation, $m = m(r)$ defines the mass function. One can modify the system by using the extended geometric deformation (EGD) on the seed metric within the source $\Theta_{\epsilon\varepsilon}$ as

$$\xi \to \varepsilon = \xi + g, \tag{13}$$
$$e^{-\varepsilon} \to e^{-\epsilon} = e^{-\lambda} + f, \tag{14}$$

where f and g reveal the geometric deformations components. One can separate the Einstein field equations by considering Eqs. (13–14) through Eqs. (5–7) into two different proposals. The first proposal of field equations is separated as:

$$\frac{1}{\mathcal{K}^2}\left[\frac{1}{r^2} - e^{-\lambda}\left(\frac{1}{r^2} - \frac{\lambda'}{r}\right)\right] = T_0^0, \tag{15}$$
$$\frac{1}{\mathcal{K}^2}\left[\frac{1}{r^2} - e^{-\lambda}\left(\frac{1}{r^2} + \frac{\xi'}{r}\right)\right] = T_1^1, \tag{16}$$
$$-\frac{e^{-\lambda}}{4\mathcal{K}^2}\left(2\xi'' + \xi'^2 - \lambda'\xi' + 2\frac{\xi' - \lambda'}{r}\right) = T_2^2. \tag{17}$$

For $\Theta_{\epsilon\varepsilon}$ sector, new developed filed equations are provided as:

$$\frac{1}{\mathcal{K}^2}\left[-\frac{f}{r^2} - \frac{f'}{r}\right] = \Theta_0^0, \tag{18}$$
$$\frac{1}{\mathcal{K}^2}\left[-X_1 - f\left(\frac{1}{r^2} + \frac{\varepsilon'}{r}\right)\right] = \Theta_1^1, \tag{19}$$
$$\frac{1}{\mathcal{K}^2}\left[-X_2 - \frac{f}{4}\left(2\varepsilon'' + \varepsilon'^2 + 2\frac{\varepsilon'}{r}\right)\right] - \frac{f'}{4\mathcal{K}^2}\left(\varepsilon' + \frac{2}{r}\right) = \Theta_2^2, \tag{20}$$

where

$$X_1 = \frac{e^{-\lambda}g'}{r}, \tag{21}$$
$$X_2 = \frac{e^{-\lambda}}{4}\left(2g'' + g'^2 + 2\frac{g'}{r} + 2\xi'g' - \lambda'g'\right). \tag{22}$$

From the above two proposals of field equations, the first part is linked with the usual energy-momentum tensor, i.e., $T_{\epsilon\varepsilon}$. The second proposal, under the control of some physical realistic condition, helps us to discuss the Θ-sector, $\Theta_{\epsilon\varepsilon}$ (ϵ, f and g). The energy exchange between these two proposals of matter $T_{\epsilon\varepsilon}$ and $\Theta_{\epsilon\varepsilon}$ [15] provides the successfully decoupled system. After the confirmation of energy exchange, one can carry the construction of a hairy BH within the scope of deformations to the Schwarzschild metric, which serves as the initial seed. The Schwarzschild metric is given by:

$$1 - \frac{2M}{r} = e^{\xi} = e^{-\lambda}. \tag{23}$$

Within the framework of deformation functions $\{f, g\}$ under the suitable choice, an event horizon from the deformed solution is defined as:

$$e^{\varepsilon(r_H)} = e^{-\lambda(r_H)} = 0, \tag{24}$$

where r_H provides the relation for the horizon radius. Within the Schwarzschild coordinates, we have the following relation

$$e^{\varepsilon} = e^{-\lambda}, \tag{25}$$

with the following constraint

$$\tilde{p}_r = -\tilde{\rho}. \tag{26}$$

Now, one can define the geometric deformation function f as

$$f = \left(1 - \frac{2M}{r}\right)\left(e^{g} - 1\right), \tag{27}$$

which leads to

$$ds^2 = \left(1 - \frac{2M}{r}\right)H(r)dt^2 - \left(1 - \frac{2M}{r}\right)^{-1}H^{-1}(r)dr^2 - r^2d\Omega^2. \tag{28}$$

We will add one more constraint to solve for the auxiliary function H. One can observe other conditions, such as strong energy conditions and dominant energy conditions, on and outside the horizon, according to groundbreaking research in Ref. [72]. It's interesting to note that BHs that are physically significant also have to meet a less stringent requirement, called the weak energy condition [73]. The main approach that needs to be taken into account in this study is the phenomenon pertaining to weak energy conditions.

$$\begin{aligned} &0 \le \tilde{\rho}, \\ &0 \le \tilde{\rho} + \tilde{p}_r, \\ &0 \le \tilde{\rho} + \tilde{p}_t. \end{aligned} \tag{29}$$

Interestingly, Eq. (26), reproduces as

$$0 \le \Theta_0^0, \tag{30}$$
$$\Theta_2^2 \le \Theta_0^0. \tag{31}$$

Now, by using Eqs. (18) and (20) the above inequalities can be revised as

$$0 \le 1 - H - (r - 2M)H', \tag{32}$$
$$0 \le 2 - 2H + 4MH' + r(r - 2M)H''. \tag{33}$$

Now, we are able to find some h satisfying (32) whenever

$$G(r) = 1 - H - (r - 2M)H', \tag{34}$$

for $G > 0$. The generic solution for the above equation reads as

$$\frac{r - c_1}{r - 2M} - \frac{1}{r - 2M}\int G(x)dx = H(r). \tag{35}$$

In the above equation, c_1 represents the constant with dimensions of length. Further, there exist an extra condition on $G(r)$ as a consequence of constraint (33) expressed as

$$0 \leq 2G - rG'. \tag{36}$$

We can say G is an arbitrary positive function, which is satisfying (36); in the current analysis, we shall consider it as

$$G(r) = \alpha \frac{M}{r^2} \ln\left(\frac{r}{\beta}\right), \tag{37}$$

now

$$1 - H - (r - 2M)H' = \alpha \frac{M}{r^2} \ln\left(\frac{r}{\beta}\right) \geq 0, \tag{38}$$

where α and β are considered constants with dimensions of a length and having the following constraint

$$0 \leq \alpha. \tag{39}$$

The exact solution of Eq. (38) is

$$H(r) = \frac{r - c_1}{r - 2M} + \frac{\alpha M}{r(r - 2M)}\left(1 + \ln\left(\frac{r}{\beta}\right)\right). \tag{40}$$

Now, we can put $c_1 = 2M$ in order to recover the Schwarzschild original solution when $\alpha \to 0$. Note that the inequality (33) is satisfied whenever

$$\ln\left(\frac{r}{\beta}\right) \geq \frac{1}{4}. \tag{41}$$

Now, replacing Eq. (40) in (28) we arrive at the following final form of solution

$$f(r) = e^{\varepsilon} = e^{-\lambda} = 1 - \frac{2M}{r} + \frac{\alpha M}{r^2} + \frac{\alpha M}{r^2} \ln\left(\frac{r}{\beta}\right). \tag{42}$$

The lapse function of the recently obtained solution under the influence of gravitational decoupling is represented by $f(r)$ in the equation above. Here are a few things we want to draw attention to. While maintaining the fundamental theory unchanged, the gravitational decoupling generalizes the Schwarzschild BH solution via an extra source $\Theta_{\epsilon\varepsilon}$ on the seed solution will be examined in this work. The solution displayed over a range of α and β parameter values exhibits the emergence of this phenomenon. The Schwarzschild BH solution is reached in the limit when α approaches zero. Moreover, further explanations in this context can be referred to Ref. [71].

3 Strong gravitational lensing and it's observable

Here, we study the strong gravitational lensing by decoupling modified BH. We intend to investigate how the decoupling modified BH parameters, α, and β influence the various astrophysical consequences due to strong gravitational lensing and compare it to the other astrophysical BH such as Schwarzschild BH ($\alpha = 0$).

To investigate the strong deflection angle of photon rays occurring in the equatorial plane ($\theta = \frac{\pi}{2}$), we rewrite the metric (42) component by the dimensionless transformation as $t \to \frac{t}{2M}, r \to \frac{r}{2M}, \alpha \to \frac{\alpha}{2M}$ and $\beta \to \frac{\beta}{2M}$ as

$$d\bar{s}^2 = -A(r)dt^2 + B(r)dr^2 + C(r)d\phi^2, \tag{43}$$

where

$$A(r) = 1 - \frac{1}{r} + \frac{\alpha \log\left(\frac{r}{\beta}\right)}{2r^2} + \frac{\alpha}{2r^2}, \tag{44}$$

$$B(r) = \left[1 - \frac{1}{r} + \frac{\alpha \log\left(\frac{r}{\beta}\right)}{2r^2} + \frac{\alpha}{2r^2}\right]^{-1}, \tag{45}$$

and

$$C(r) = r^2. \tag{46}$$

The strong deflection angle and the lens equation govern the strong gravitational lensing phenomenon. The null geodesic equation can be interpreted as follows:

$$\dot{r} = \frac{dr}{d\tau} = \sqrt{E^2 - \frac{L^2}{r^2}A(r)}, \tag{47}$$

where the energy of test particle $E = -p_\mu \xi_t^\mu$ and angular momentum $L = p_\mu \xi_\phi^\mu$ of the particle and the function $A(r)$ is given by the Eq. (44). For the unstable photon circular orbit of radius r_{ph}, the conditions for the effective potentials are $\frac{dV_{eff}}{dr}|_{r_{ph}} = 0$ and $\frac{d^2V_{eff}}{dr^2}|_{r_{ph}} < 0$. Thus, the radius of the photon sphere r_{ph} is the biggest real root of the following equation

$$2A(r_{ph}) - r_{ph}A'(r_{ph}) = 0. \tag{48}$$

The photon sphere radius r_{ph} with the decoupling modified BH parameters α and β is displayed in Fig. 1a. It is observed that for the lowest value of β, the photon sphere radius, r_{ph}, is maximum with the parameter α. It reaches its maximum value ($r_{ph} = 1.5$), corresponds to the case of the Schwarzschild BH, but for the lowest value of α, the photon sphere radius r_{ph} is maximum with the parameter α.

When the particles reach the closest distance $r = r_0$ to the central BH, where $\frac{dr}{d\tau} = 0$, one can consider the minimum impact parameter, denoted as u_0, in terms of the minimum distance r_0 [70].

$$u_0 = \frac{r_0}{\sqrt{A(r_0)}}. \tag{49}$$

The critical impact parameter for the unstable photon orbit u_{ph} with the framework of decoupling modified BH is given by

$$u_{ph} = \frac{r_{ph}}{\sqrt{A(r_{ph})}}, \tag{50}$$

and its behavior with the decoupling modified BH parameters α and β is shown in Fig. 1b.

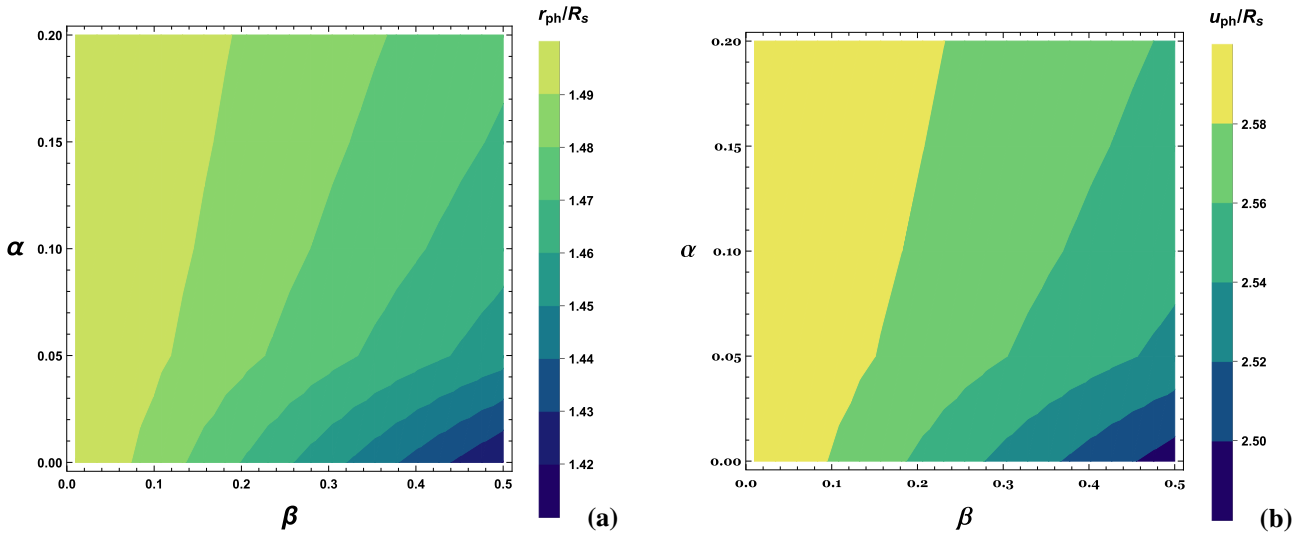

Fig. 1 The photon sphere radius r_{ph}/R_s (left panel **a**); and the impact parameter u_{ph}/R_s (right panel **b**) as a function of decoupling modified BH parameters α and β

The strong deflection angle in the spacetime of a decoupling modified BH expressed as a function of the closest approach distance denoted as r_0, can be expressed as follows [74]:

$$\alpha_D = I(r_0) - \pi = 2\int_{r_0}^{\infty} \frac{\sqrt{B(r)}dr}{\sqrt{C(r)}\sqrt{\frac{A(r_0)C(r)}{A(r)C(r_0)} - 1}} dr - \pi. \tag{51}$$

The strong deflection angle, denoted as $\alpha_D(r_0)$, is influenced by the connection between r_0 and r_{ph}. It demonstrates an elevation when these two values are roughly equivalent (i.e., $r_0 \approx r_{ph}$). So, we define a new variable z as [70]

$$z = 1 - \frac{r_0}{r}. \tag{52}$$

When r_0 is approximately equal to r_{ph}, the deflection angle assumes the following form [75–79]

$$\alpha_D(u) = -\bar{a}\ \log\left(\frac{u}{u_{ph}} - 1\right) + \bar{b} + \mathcal{O}((u - u_{ph}) \times \log(u - u_{ph}), \tag{53}$$

where

$$\bar{a} = \frac{2r_{ph}}{\sqrt{\alpha + 4r_{ph}^2 - 4\alpha \log\left(\frac{r_{ph}}{\beta}\right)}},$$

and

$$\bar{b} = b + I_R(r_{ph}), \tag{54}$$

with

$$b = -\pi + \frac{2r_{ph}}{\sqrt{\alpha + 4r_{ph}^2 - 4\alpha \log\left(\frac{r_{ph}}{\beta}\right)}} \times \log\left[\frac{\alpha + 4r_{ph}^2 - 4\alpha \log\left(\frac{r_{ph}}{\beta}\right)}{2r_{ph}^2 - 2r_{ph} - \alpha \log\left(\frac{r_{ph}}{\beta}\right)}\right],$$

$$I_R(r_{ph}) = 2\int_0^1 \left(r_{ph}\left[\sqrt{\frac{B(z)}{C(Z)}}\left(\frac{A(r_{ph})}{C(r_{ph})}\frac{C(z)}{A(z)} - 1\right) \times \frac{1}{(1-z)^2}\right] - \frac{\bar{a}}{z\, r_{ph}}\right)dz, \tag{55}$$

which is obtained numerically.

We numerically estimate the strong lensing coefficients, the critical impact parameter u_{ph}, deflection angle coefficients $\bar{a}$ and $\bar{b}$ at $r = r_{ph}$ with decoupling modified BH parameters $\alpha = 0.1, 0.2, 0.3, 0.4, 0.5$ and $\beta = 0.2, 0.4, 0.6$ and which is given in Table 1.The behaviour of the strong lensing coefficients u_{ph}, $\bar{a}$ and $\bar{b}$ have been shown in Figs. 1b, 2a, b; and Table 1.

In Table 1 and Fig. 1b, it is seen that for the fixed value of the parameter β, the critical impact parameter u_{ph}/R_s decreases with the parameter α while for the fixed value of the parameter α the critical impact parameter u_{ph}/R_s increases with the parameter β. However for the lowest value of the parameter β the critical impact parameter u_{ph}/R_s reaches its maximum value ($u_{ph}/R_s = 2.59808$) and which also corresponds to the case of the Schwarzschild BH but decreases with the parameter α and reaches its maximum value ($u_{ph}/R_s = 2.59808$) corresponds to the case of the Schwarzschild BH [70] but for the lowest value of α, the critical impact parameter u_{ph}/R_s is minimum with the parameter β. In Fig. 2a, b, it is observed that for the lowest value of the parameter α, deflection angle coefficients $\bar{a}$ and $\bar{b}$ reach their maximum value with the parameter β and β, deflection angle coefficients $\bar{a}$ and $\bar{b}$ reach their lowest value with the

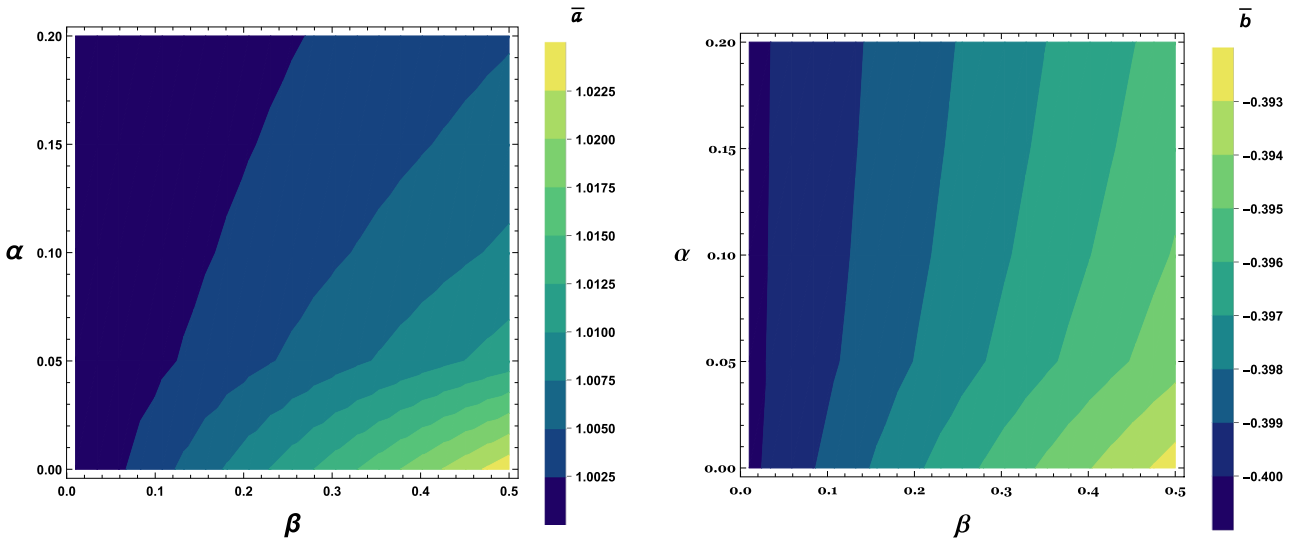

Fig. 2 The behaviour of the deflection limit coefficient $\bar{a}$ (left panel **a**); and the deflection limit coefficient $\bar{b}$ (right panel **b**) as a function of decoupling modified BH parameters α and β

Table 1 Estimation of strong lensing coefficients with decoupling modified BH parameters $\alpha = 0.1, 0.2, 0.3, 0.4, 0.5$ and $\beta = 0.2, 0.4, 0.6$

β	Strong lensing coefficients			
	α	$\bar{a}$	b	u_{ph}/R_{sh}
Schwarzschild BH	0	1	− 0.40023	2.59808
	0.1	1.05185	− 0.369879	2.31356
	0.2	1.16183	− 0.330424	1.95377
0.2	0.3	2.22856	− 0.965544	1.29196
	0.4	0.356304	− 1.06028	0.176516
	0.5	0.238526	− 1.79452	0.0973293
	0.1	1.02752	− 0.373254	2.3862
	0.2	1.06516	− 0.332416	2.14678
0.4	0.3	1.11795	− 0.256123	1.86519
	0.4	1.173	− 0.0430559	1.51141
	0.5	1.02367	− 0.476603	1.05225
	0.1	1.01565	− 0.375937	2.42628
	0.2	1.03251	− 0.341942	2.24116
0.6	0.3	1.04837	− 0.290884	2.0398
	0.4	1.05608	− 0.209392	1.81913
	0.5	1.03738	− 0.0835361	1.57815

parameter α. The behaviour of deflection angle α_D in the strong field limit decoupling modified BH parameters α and β are shown in Fig. 3a–c. In Fig. 3a, it is observed that for the lowest value of the parameter α, the strong deflection angle α_D reaches its maximum value with the parameter β. For the lowest value of the parameter β, strong deflection angle α_D reaches its minimum value with the parameter α. In Fig. 3a, b, it is also observed that for the lowest value of the parameter α, deflection angle α_D decreases with the critical parameter u with different value of β and the fixed value of the parameter α; and decreases with the critical parameter u with different value of α and the fixed value of the parameter β. In Fig. 3a, b, it is also observed that $\alpha_D \to \infty$ as $u \to u_{ph}$ i.e strong deflection angle α_D diverges when $u \to u_{ph}$. In Fig. 3b, further, it is also seen that the strong deflection angle α_D for the decoupling modified BH is smaller compared to the Schwarzschild BH ($\alpha = 0$).

3.1 Lensing observables

In this discussion, we explore the examination of various observable aspects of strong gravitational lensing within the

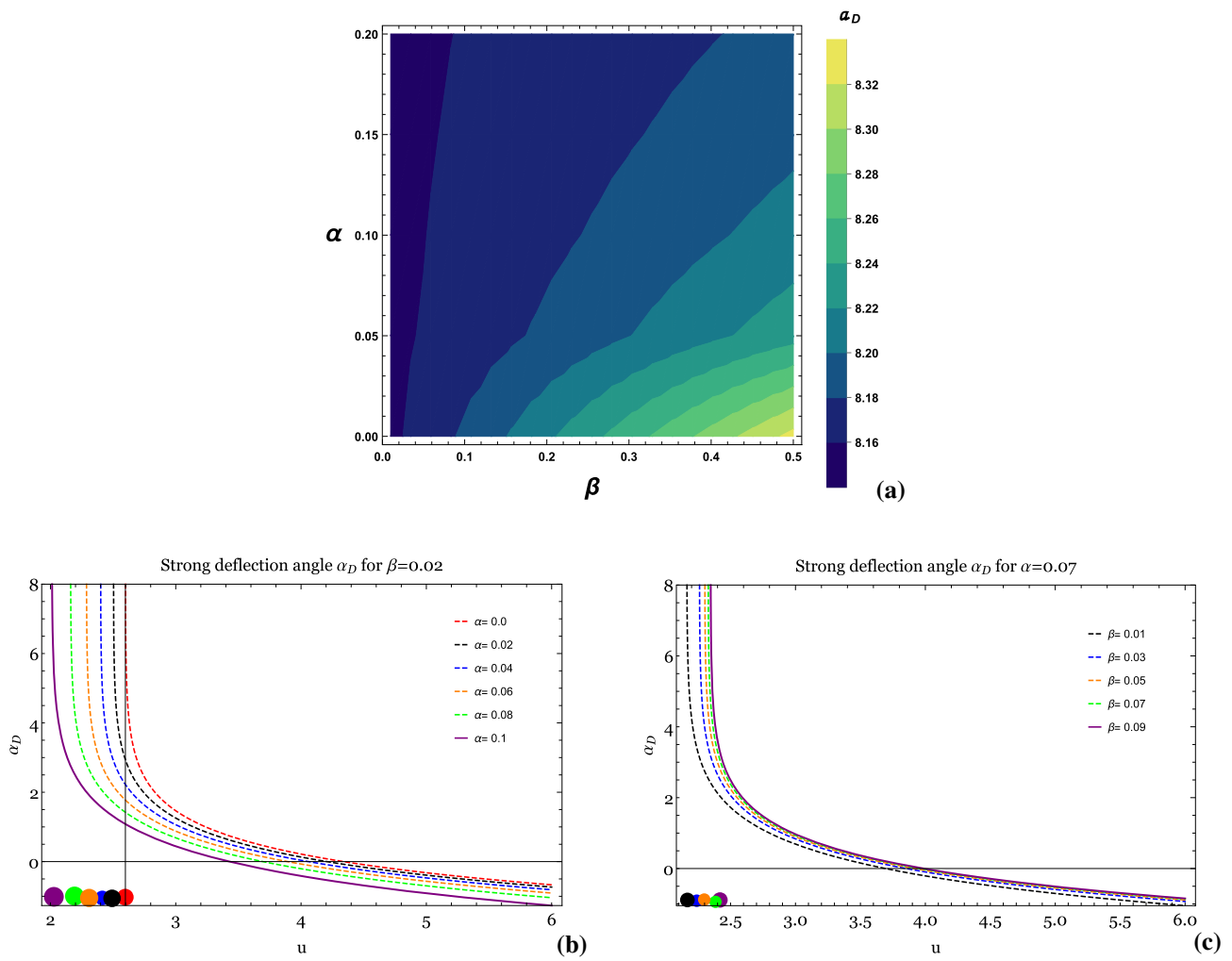

Fig. 3 The deflection angle α_D (left panel **a**) as a function of decoupling modified BH parameters α and β and the deflection angle α_D as a function of critical parameter u with different value of α for the fixed, β (panel **b**) and with different value of β for the fixed, α (panel **c**). The dots in right panels **b**, **c** represent the values of the critical impact parameter $u = u_{ph}$, where the deflection angle α_D becomes divergent

framework of a decoupling-modified black hole. To facilitate this exploration, we consider a scenario in which both the observer and the source are situated at a considerable distance from the BH (the lens), and their alignment is nearly perfect. Furthermore, we assume the source is positioned behind the BH (lens). Consequently, we define the lens equation as follows [80]:

$$\tilde{\beta} = \theta - \frac{D_{ls}}{D_{os}}\Delta\alpha_n, \tag{56}$$

where $\Delta\alpha_n = \alpha_D(\theta) - 2n\pi$ represents the offset deflection angle. Here, $\alpha_D(\theta)$ is the primary deflection angle, and n denotes the number of revolutions or loops that a photon ray completes around the BH. The angles $\tilde{\beta}$ and θ correspond to the angular separations between the BH (lens) and the source and between the observer and the source, respectively. The distances D_{ol}, D_{ls}, D_{os} represent the observer-lens, lens-source, and observer-source distances, respectively, with the relationship $D_{os} = D_{ol} + D_{ls}$.

Using Eq. (51) and Eq. (56), the angular separation between the BH (lens) to the n^{th} relativistic image can be written as

$$\theta_n = \theta_n^0 - \frac{u_{ph}e_n(\theta_n^0 - \beta)D_{os}}{\bar{a}D_{ol}D_{ls}}, \tag{57}$$

where

$$e_n = e^{\frac{\bar{b}-2n\pi}{\bar{a}}},$$
$$\theta_n^0 = \frac{u_{ph}(1+e_n)}{D_{ol}}.$$

Here, θ_n^0 denotes the angular position of the image when a photon completes a total of $2n\pi$ rotations around the BH (lens).

In the realm of strong gravitational lensing, where surface brightness is conserved, the magnification of the relativistic effect can be defined as the ratio of the solid angle covered by the n-th image to that covered by the source [36]. To determine the magnification for the n-th relativistic image, we can derive it as in [70].

$$\mu_n = \left(\frac{\tilde{\beta}}{\theta}\frac{d\tilde{\beta}}{d\theta}\right)^{-1}\Big|_{\theta_0} = \frac{u_{ph}^2(1+e_n)e_n D_{os}}{\tilde{\beta}\bar{a}D_{ls}D_{ol}^2}. \tag{58}$$

The above equation strongly implies that the first relativistic image exhibits the highest brightness level, and the magnification decreases exponentially with increasing 'n'. In simpler terms, the brightness of this initial image exceeds that of the subsequent relativistic images. Noteworthy is that Eq. (58) becomes unbounded as $\tilde{\beta} \to 0$, indicating that perfect alignment maximizes the possibility of detecting relativistic images. Here, we examine the case where the brightest image, specifically the outermost image θ_1, is resolved as a single image, while the remaining inner images are packed together at θ_∞. ($\theta_n|_{n\to\infty} =: \theta_\infty$). Using the deflection angle provided in equation (53), one can determine various strong lensing observables. These include the angular position of the set of images θ_∞, the angular separation between the outermost and innermost images S, and the relative magnification r_{mag} between the outermost relativistic image and the other set of inner relativistic images [58,70].

$$\theta_\infty = \frac{u_{ph}}{D_{ol}}, \tag{59}$$

$$S = \theta_1 - \theta_\infty \approx \theta_\infty e^{\frac{(\bar{b}-2\pi)}{\bar{a}}}, \tag{60}$$

$$r_{mag} = \frac{\mu_1}{\Sigma_{n=2}^{\infty}\mu_n} \approx \frac{5\pi}{\bar{a}log(10)}. \tag{61}$$

If the strong lensing observables θ_∞, S, and r_{mag} can be measured from the observations, the strong lensing coefficients $\bar{a}$, $\bar{b}$ and the critical impact parameter u_{ph} can be obtained easily by the equations (59), (60) and (61). These obtained values can then be further compared with theoretically estimated values, thereby providing a robust validation framework for our theoretical predictions in the context of strong gravitational lensing by decoupling modified BHs. Future telescopes and observational technologies play a crucial role in testing theoretical predictions, especially in the context of strong gravitational lensing by decoupling modified BHs Future telescopes and observational technologies enable the precise measurement of strong lensing observables, facilitating the comparison with theoretical predictions based on the gravitational decoupling framework. This comparison forms the basis of a validation framework, allowing for the empirical testing and refinement of theoretical models in the context of strong gravitational lensing by decoupling modified BHs. Furthermore, Using these findings, one can identify the nature of the decoupling modified BHs and Schwarzschild BHs and finally distinguish between them.

Exploring supermassive BHs at the center of neighboring galaxies, namely $M87^*$, $SgrA^*$, and $NGC4649$, we perform numerical assessments of strong lensing observables θ_∞, S, and r_{mag} within the framework of a decoupling modified BH (see in Table 2). Their mass and distance from the earth for $M87^*$ are approximately as $M \approx 6.5 \times 10^9 M_\odot$ and $d_{ol} \approx 16.8$ Mpc [81]; for $SgrA^*$ the corresponding values are approximately as $M \approx 4.28\times10^6 M_\odot$ and $d_{ol} \approx 8.32$ kpc [82] and for $NGC4649$,the mass and distance are approximately as $M \approx 4.72 \times 10^9 M_\odot$ and $d_{ol} \approx 16.46 Mpc$ as documented in [83]. We numerically estimate the strong lensing observables θ_∞, S, and r_{mag} in the context of $M87^*$ and $SgrA^*$ supermassive BHs with decoupling modified BH parameters $\alpha = 0.01, 0.02, 0.03, 0.04, 0.05$ and $\beta = 0.02, 0.04, 0.06$ and which is given in Table 2. The behaviour of the strong lensing observables θ_∞, S, and r_{mag} have been shown in Figs. 4, 5 and 6; and Table 2. In Table 2 and Fig. 4a, b, it is seen that for the fixed value of the parameter, β the observable quantity angular position of the relativistic image θ_∞ decreases with the parameter α while for the fixed value of the parameter α the observable quantity θ_∞ increases with the parameter β. However for the lowest value of the parameter β, the observable quantity θ_∞ reaches its maximum value with the parameter α and for the lowest value of α, the observable quantity θ_∞ is minimum with the parameter β. In Fig. 5a, b, it is observed that for the fixed value of the parameter, β, the observable quantity angular separation of the relativistic images S increases with the parameter α while for the fixed value of the parameter α the observable quantity θ_∞ decreases with the parameter β. However, for the lowest value of the parameter, α, the observable quantity S reaches its maximum value with the parameter β, but the lowest value of the parameter β, the observable quantity S, is the minimum with the parameter α. In Table 2 and Fig. 6, Further, it is observed that for the fixed value of the parameter, β, the observable quantity relative magnification of the relativistic image r_{mag} decreases with the parameter α while for the fixed value of the parameter α the observable quantity r_{mag} increases with the parameter β. However, for the lowest value of the parameter, β, the observable quantity r_{mag} reaches its maximum value with the parameter α and for the lowest value of α, the observable quantity θ_∞ is minimum with the parameter β. It is observed that the relative magnification of the relativistic images r_{mag} for decoupling modified BH is smaller than corresponds to the case of the Schwarzschild BH ($r_{mag} = 6.82188$ magnitude) [70]. Additionally, it is observed that the relative magnification r_{mag} for the relativistic images remains independent of the mass or distance of the BHs.

We also compare the observable quantities in between Schwarzschild and decoupling modified BHs (see Tables

Table 2 Estimation of lensing observable quantities for supermassive BHs $M87^*$, $SgrA^*$, $NGC7457$as a function of decoupling modified BH parameters $\alpha = 0.01, 0.02, 0.03, 0.04, 0.05$ and $\beta = 0.02, 0.04, 0.06$.The relative magnification r_{mag} does not depend on the BH mass or BH distance from the observer

β	Parameters		$M87^*$		$SgrA^*$		$NGC4649$	$M87^*$, $SgrA^*$, $NGC4649$
	α	θ_∞ (μas)	S (μas)	θ_∞ (μas)	S (μas)	θ_∞ (μas)	S (μas)	r_{mag}
	0	19.8216	0.0248067	26.3826	0.0330177	14.6906	0.0183856	6.82188
	0.01	19.4644	0.0260429	25.907	0.0346631	14.4261	0.0193018	6.75735
	0.02	19.0943	0.0274816	25.4144	0.036578	14.1518	0.0203681	6.6864
0.02	0.03	18.7097	0.0291779	24.9026	0.0388358	13.8668	0.0216253	6.60778
	0.04	18.3088	0.0312086	24.369	0.0415387	13.5697	0.0231304	6.51982
	0.05	17.8891	0.0336851	23.8104	0.0448348	13.2585	0.0249658	6.42032
	0.01	19.5118	0.0258091	25.9702	0.0343519	14.4612	0.0191285	6.76875
	0.02	19.1928	0.0269454	25.5456	0.0358643	14.2248	0.0199706	6.71129
0.04	0.03	18.8638	0.0282447	25.1077	0.0375936	13.9809	0.0209336	6.64881
	0.04	18.5235	0.0297453	24.6548	0.039591	13.7288	0.0220458	6.58047
	0.05	18.1708	0.0314986	24.1853	0.0419246	13.4674	0.0233453	6.50517
	0.01	19.5394	0.0256749	26.007	0.0341732	14.4817	0.019029	6.77535
	0.02	19.2499	0.0266442	25.6216	0.0354634	14.2671	0.0197474	6.72549
0.06	0.03	18.9524	0.0277336	25.2257	0.0369134	14.0467	0.0205548	6.67186
	0.04	18.6463	0.0289672	24.8182	0.0385553	13.8197	0.0214691	6.61392
	0.05	18.3305	0.0303761	24.3979	0.0404306	13.5857	0.0225133	6.55098

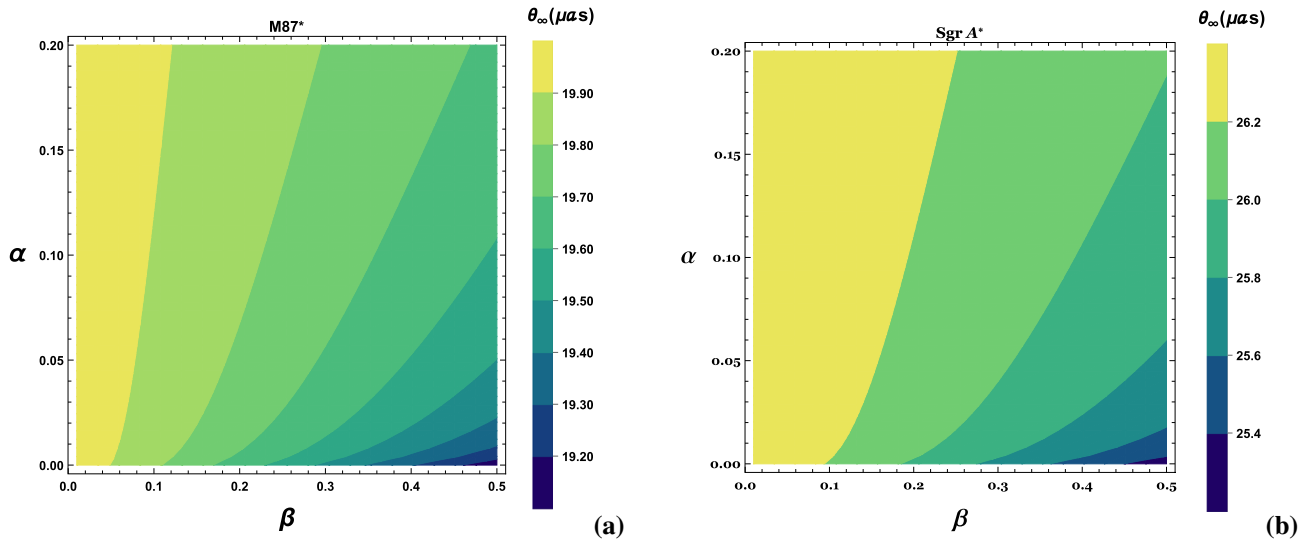

Fig. 4 The angular image position θ_∞ as a function of decoupling modified BH parameters α and β for $M87^*$ (left panel **a** and for $SgrA^*$ (right panel **b**)

1, 2). In Table 2, by considering the supermassive BH $M87$ at the centre of the galaxy, it is observed in our Estimation that the angular position of innermost images θ_∞ in the context of decoupling modified BH is significantly smaller than corresponds to the case of the Schwarzschild BH ($\theta_\infty = 19.8216\,\mu as$ [70]. Also, the decoupling modified BH has larger image separation S and smaller relative magnification r_{mag} compared to the case of the Schwarzschild BH ($S = 0.0248067\,\mu as$, $r_{mag} = 6.82188$ magnitude) [70]. The difference value of the strong lensing observables θ_∞, S, and r_{mag} for the decoupling modified BH ($\beta = 0.02, \alpha = 0.05$) from the Schwarzschild BH ($\alpha = 0$) respective as $\sim 1.9325\,\mu as$ $\sim 0.0088784\,\mu as$ and ~ 0.40156 magnitude. It suggests that the outermost relativistic images for the decoupling modified BH are very close to the innermost relativistic images, which may be separated from the other astrophysical BH images. In addition, if the outermost relativistic image can be resolved, we will distinguish the decoupling

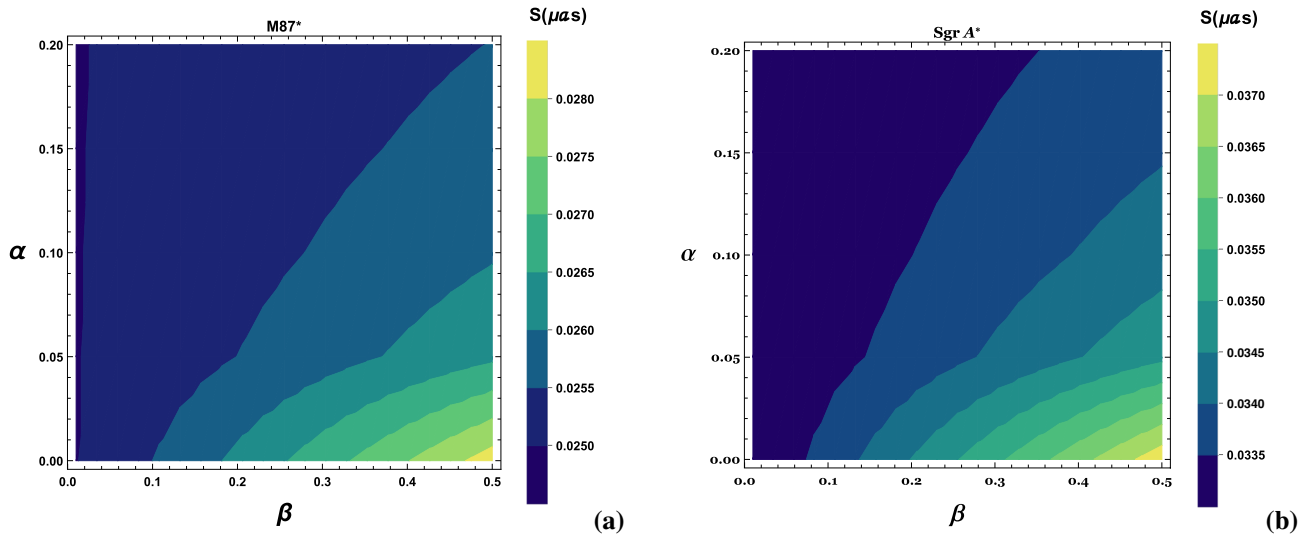

Fig. 5 The angular image separation S as a function of decoupling modified BH parameters α and β for $M87^*$ (left panel **a**) and for $Sgr A^*$ (right panel **b**)

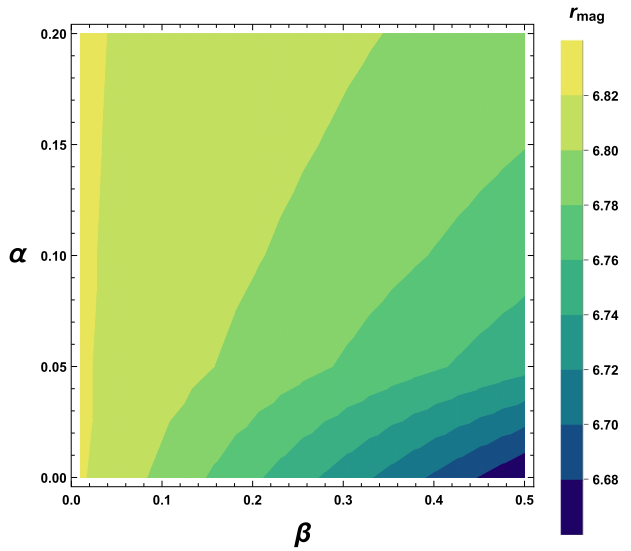

Fig. 6 The relative magnification r_{mag} as a function of decoupling modified BH parameters α and β.Note that the relative magnification r_{mag} does not depend on the mass or distance of the BH from the observer

of modified BHs from a Schwarzschild BH is using the new existing technology. However, the difference of S from the Schwarzschild is not more than $0.009\,\mu as$, which makes the task of discriminating decoupling modified BHs via strong gravitational lensing observation much more difficult.

In mapping out the future trajectory of this study, we could propose specific experiments that leverage current or forthcoming telescopes to validate the predictions of the gravitational decoupling framework in strong gravitational lensing scenarios. Additionally, suggesting theoretical refinements, conducting numerical simulations, performing comparative analyses with alternative theories, and fostering interdisciplinary collaborations could deepen our understanding and refine the framework's applicability. By delineating these approaches, we can offer a clear roadmap for future research aimed at advancing the comprehension and testing of the gravitational decoupling framework within the context of strong gravitational lensing.

However, the decoupling modified BHs could be quantitatively distinguished from other astrophysical BHs, such as Schwarzschild BHs.

3.2 Einstein ring

In the scenario where the source, BH (lens), and observer are perfectly aligned, denoted by $\tilde{\beta} = 0$, the BH deflects light rays in all directions. This deflection results in the formation of a ring-shaped image, commonly referred to as an Einstein ring [84–89].

Simplifying Eq. (57) for $\beta = 0$, we derive the angular radius of the nth relativistic image as follows:

$$\theta_n = \theta_n^0\left(1 - \frac{u_{ph} e_n D_{os}}{\bar{a} D_{ls} D_{ol}}\right). \tag{62}$$

Considering the case when the BH (lens) is positioned at the halfway point between the source and receiver, specifically $D_{os} = 2D_{ol}$, and with the assumption of $D_{ol} \gg u_{ph}$, the angular radius of the n^{th} relativistic Einstein ring in the context of decoupling modified BHs is expressed as follows:

$$\theta_n^E = \frac{u_{ph}(1 + e_n)}{D_{ol}}. \tag{63}$$

The radius of the outermost Einstein ring θ_1^E is shown in Fig. 7 for the supermassive BHs $M87^*$ (Fig. 7a, b) and $Sgr A^*$

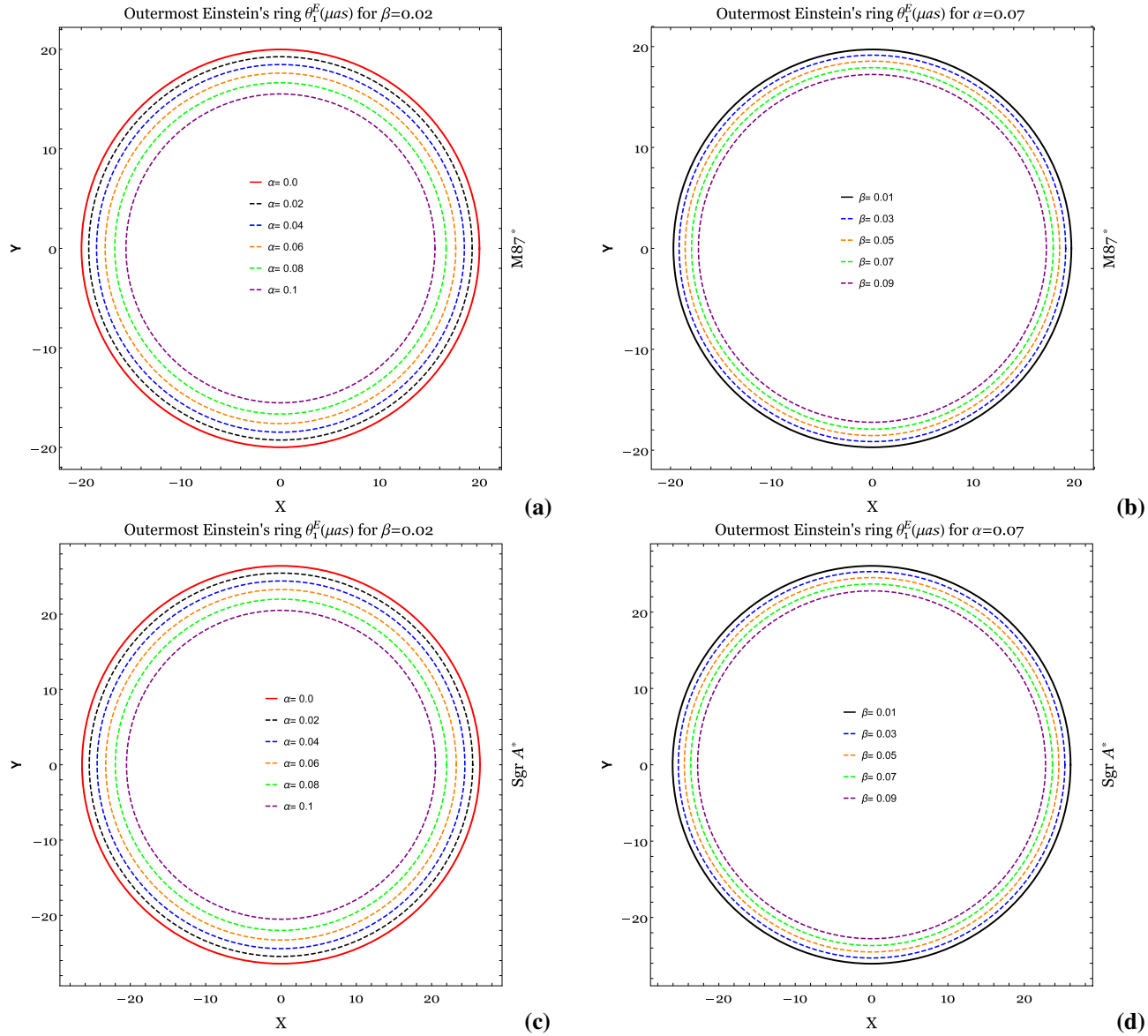

Fig. 7 The outermost Einstein's ring θ_I^E as decoupling modified BH parameter α for the fixed value of β in the context of $M87^*$ (panel **a**, **b**) and $Sgr A^*$ (panel **c**, **d**) for $Sgr A^*$ respectively.The solid red circular ring corresponds to the case of Schwarzschild's BH

(Fig. 7c, d). From these figures, it is observed that for the fixed value of the parameter, β, the radius of the outermost Einstein ring θ_1^E decreases with the parameter α and also for the fixed value of the parameter α the radius of the outermost Einstein ring θ_1^E decreases with the parameter β. The angular radius θ_1^E of the outermost Einstein ring in the context of decoupling modified BH is smaller than the corresponding case of the standard Schwarzschild BH $\alpha = 0$.

3.3 Time delay in strong field limit

Time delay is another most important observable in the context of the strong gravitational lensing phenomenon. It is derived from the temporal gap between the formation of two relativistic images, stemming from the distinct paths the photons traverse around the BH. The diverse photon trajectories for different relativistic images lead to varying time travels, resulting in time differences between them. By discerning the time signals of these relativistic images during observations, it becomes possible to calculate the time delay between the two signals [90]. The time taken by a photon to complete a revolution around the BH is detailed in [90].

$$\tilde{T} = \tilde{a} log\left(\frac{u}{u_{ph}} - 1\right) + \tilde{b} + \mathcal{O}(u - u_{ph}). \tag{64}$$

Utilizing the expression provided in Eq. (64), one can calculate the time difference between two relativistic images.

Table 3 Estimation of time delay for various supermassive BHs in the context of Schwarzschild, decoupling modified BH respectively are taken in solar mass and Mpc units, time delays $\Delta T_{2,1}$ are estimated in minutes

Galaxy	$M(M_\odot)$	$D_{ol}(Mpc)$	$\Delta T_{2,1}$ Schwarzschild BH ($\alpha = 0$)	$\Delta T_{2,1}$ decoupling modified BH ($\beta = 0.3, \alpha = 0.4$)
Milkyway	4.3×10^6	0.0083	11.4968	4.83754
M87	6.5×10^9	16.68	17378.9	7312.56
NGC 4026	1.80×10^8	13.35	481.261	202.502
NGC 7457	8.95×10^6	12.53	23.9294	10.0688
NGC 4395	3.6×10^5	4.3	0.962522	0.405003
NGC 2778	1.45×10^7	23.44	38.7682	16.3126
NGC 3379	4.16×10^8	10.70	1112.25	468.004
NGC 3607	1.37×10^8	22.65	366.293	154.126
NGC 3842	9.09×10^9	92.2	24303.7	10226.3
NGC 4261	5.29×10^8	32.36	1414.37	595.13
NGC 4486A	1.44×10^7	18.36	38.5009	16.2001
NGC 4649	4.72×10^9	16.46	12619.7	5310.04
NGC 4751	2.44×10^9	32.81	6523.76	2745.02
NGC 5077	8.55×10^8	38.7	2285.99	961.883
NGC 5516	3.69×10^9	55.3	9865.85	4151.28
NGC 5576	2.73×10^8	25.68	729.912	307.127
NGC 6251	6.14×10^8	108.4	1641.63	690.755
NGC 6861	2.10×10^9	28.71	5614.71	2362.52
NGC 7052	3.96×10^8	70.4	1058.77	445.504
NGC 7768	1.34×10^9	116.0	3582.72	1507.51
Cygnus A	2.66×10^9	242.7	7111.95	2992.52

In the context of a spherically static symmetric BH spacetime, the time delay between two relativistic images, particularly when these images reside on the same side of the BH, is determined as follows:

$$\Delta T_{2,1} = 2\pi u_{ph} = 2\pi D_{ol}\theta_\infty. \tag{65}$$

Using the above Eq. (65), if we estimated the time delay and critical impact parameter with some negligible error, we can obtain the distance of the decoupling modified BH with some negligible error. In this paper, we estimate the time delay between images generated by strong field lensing due to decoupling modified BH in the context of various supermassive BHs in the centre nearby the galaxies (see Table 3).

Furthermore, the deviation of time delays $\delta\Delta T_{2,1} = \Delta T_{2,1}^{Schwarzschild\ BH} - \Delta T_{2,1}^{decoupling\ modified\ BH}$ for decoupling modified BH from the Schwarzschild BH has been shown in Fig. 8a, b. From these two figures, it is observed that for the lowest value of the parameter α, the deviation of time delays $\delta\Delta T_{2,1}$ reaches its maximum value with the parameter β and for the lowest value of the parameter β, the deviation of time delays $\delta\Delta T_{2,1}$ reaches its minimum value with the parameter α.

4 Results and discussions

The Event Horizon Telescope (EHT) Collaboration recently captured groundbreaking images of the supermassive BHs M87* and Sgr A* at a wavelength of 1.3 mm, achieving an unprecedented angular resolution of 20 μas [81]. While these images confirm the alignment of the observed shadow with the predictions of general relativity (GR), they also highlight the limited insight they offer into alternative gravity theories. This opens avenues for exploring alternative possibilities or modifications to GR. In this context, the concept of decoupling modified BHs, defined by a metric that encompasses a broader range of solutions compared to Schwarzschild BHs (which represent a specific case when $\alpha = 0$), becomes particularly pertinent. The decoupling modified BH is a new type hairy BH [71], which treated by the parameters α and β. Because of the decoupling of modified BH parameter α and β, can impact gravitational lensing and offer a way to distinguish a decoupling of modified BH from Schwarzschild's BH. This distinction is crucial for verifying if astrophysical BH candidates align with Einstein's predictions in GR or decoupling theory. The astrophysical BHs like Schwarzschild BHs are the special solution of decoupling

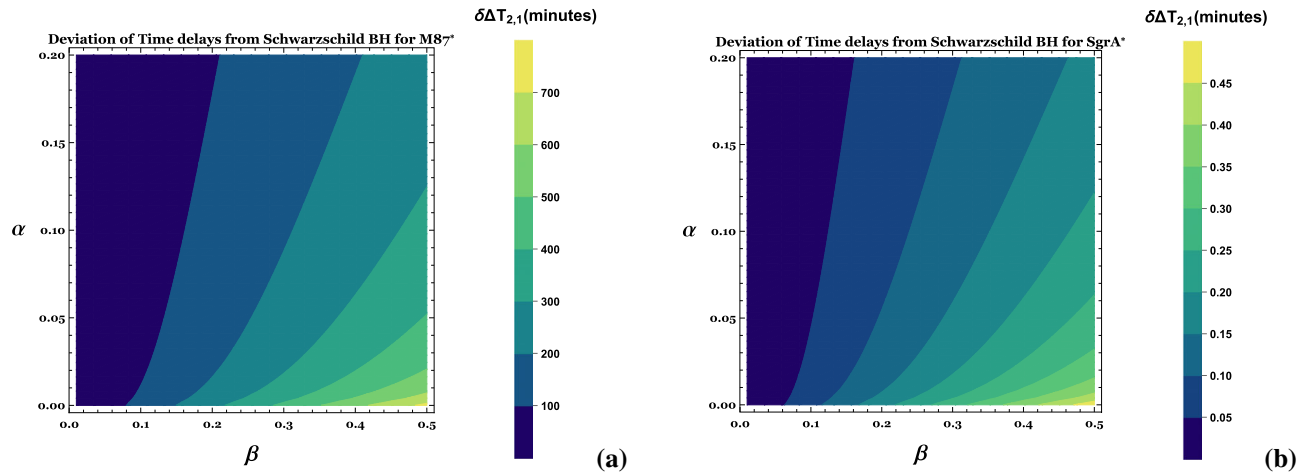

Fig. 8 The deviation of time delays for decoupling modified BH from Schwarzschild BH $\Delta T_{2,1} = T^{Sch}_{2,1} - T^{DMB}_{2,1}$ minutes for the case of $M87^*$ (panel **a**) and for $SgrA^*$ (panel **b**) with the decoupling modified BH parameters α and β

of modified BH. Numerous studies have explored gravitational lensing effects within the context of various types of BHs, as discussed previously [58,65–67,91–98]. In a related study, Kumar et al. [55] explored the strong gravitational lensing effects generated by "hairy" BHs within the Horndeski theory of gravity. They examined the astrophysical consequences across various supermassive BH scenarios influenced by the presence of "hair" in the BH solutions, contrasting them with the standard Schwarzschild BHs in general relativity. Additionally, Islam et al. [96] investigated the strong gravitational lensing effects caused by Bardeen BHs within the framework of four-dimensional Einstein-Gauss Bonnet gravity (EGB). They analyzed the astrophysical implications of these lensing effects using various supermassive BH examples with 4D EGB Bardeen BHs, comparing them with both Schwarzschild and Bardeen BH scenarios. Furthermore, Kumar et al. [58] explored gravitational lensing effects by regular electrically charged (REC) BH spacetimes, including those with and without horizons, within the strong field regime. They investigated the astrophysical consequences of these regular spacetimes across various supermassive BH scenarios, comparing them with standard Schwarzschild BHs. Recently, Vachher et al. [99] studied the strong gravitational lensing phenomena by a static spherically symmetric charged BH immersed in the perfect fluid dark matter. In this work, we investigate the strong gravitational phenomena in the context of a new type of spherically symmetric hairy BH developed by gravitational decoupling by utilizing the Bozza's [70] method. We investigate the various astrophysical consequences by taking some supermassive BHs in the centre nearby galaxies in the context of decoupling modified BH and compared it with the Schwarzschild BHs. We can see that the decoupling of modified BH parameters α and β have a significant effect on the strong gravitational observation.

(a) Strong deflection angle α_D. It is observed that for a specific value of the parameter α, the strong deflection angle α_D due to the decoupling of modified BHs (BH) increases with the parameter β (as shown in Fig. 3a, c). Thus, the presence of the parameter β greatly intensifies the gravitational bending effect compared to other BHs such as Schwarzschild BHs (as depicted in Fig. 3a). This result indicates that the gravitational lensing effect due to the decoupling of modified BHs is significantly enhanced compared to other astrophysical BHs like Schwarzschild BHs. Consequently, the decoupling of modified BHs in the presence of moving fluid and sound waves can be more easily detected and distinguished from other astrophysical BHs.

(b) Angular position θ_∞ *for the set of images.* We have numerically obtained the angular positions of the relativistic images for three supermassive BHs for the decoupling modified BH. The results obtained for the supermassive BHs $M87^*$, $SgrA^*$ and $NGC4649$ are presented in Table 2. As shown in Table 2, the innermost angular position θ_∞ is dependent on the values of the parameters α and β for decoupling modified BHs. An increase in the value of α from 0.01 to 0.05 results in a decrease in θ_∞ for BHs $M87^*$, $SgrA^*$, and $NGC4649$, while keeping β fixed. Conversely, when β increases from 0.02 to 0.06, θ_∞ increases for a fixed value of α. Notably, it is observed that for the lowest value of β, the observable quantity θ_∞ reaches its maximum value with respect to α. Furthermore, under the same mass and distance conditions for the BH, it is noted that the angular position of the innermost images, θ_∞, for decoupling modified BHs is smaller than that for Schwarzschild BHs. This implies a significant effect of decoupling modified BHs on strong lensing observables, particularly the angular position of the innermost image θ_∞, enabling the distinction of these images from those associated with Schwarzschild BHs.

(c) The angular separation. The angular separation S values between outermost and innermost relativistic images are presented for the three supermassive BHs $M87^*$, $SgrA^*$ and $NGC4649$ in Table 2. As shown in Table 2, the image separation S is dependent on the values of the parameters α and β for decoupling modified BHs. An increase in the value of α from 0.01 to 0.05 results in a inecrease in θ_∞ for BHs $M87^*$, $SgrA^*$, and $NGC4649$, while keeping β fixed. Conversely, when β increases from 0.02 to 0.06, S increases for a fixed value of α. Notably, it is observed that for the lowest value of α, the observable quantity S reaches its maximum value with respect to β. Furthermore, under the same mass and distance conditions for the BH, it is noted that the angular image separation S, for decoupling modified BHs is greater than that for Schwarzschild BHs.The difference in separation S from the Schwarzschild BH is approximately 0.01 μas, which is very small. This indicates that the outermost images for the decoupling modified BH are very close to the innermost images, making them distinguishable from images associated with other BHs.

(d) Relative magnification. As depicted in Table 2, the relative magnification r_{mag} depends on the values of the parameters α and β for decoupling modified BHs. Increasing α from 0.01 to 0.05 results in a decrease in r_{mag} for the supermassive BHs, with β held constant. Conversely, an increase in β from 0.02 to 0.06 leads to an increase in r_{mag} for a fixed value of α. Notably, for the lowest value of β, the observable quantity r_{mag} reaches its maximum value with respect to α. Furthermore, it's observed that the relative magnification r_{mag} for decoupling modified BHs is smaller than that for Schwarzschild BHs. This highlights the significant effect of decoupling modified BHs on strong lensing observables, particularly the relative magnification r_{mag}, allowing for the distinction of these images from those associated with Schwarzschild BHs. Hence, the presence of decoupling modified BHs influences the observable relative magnification r_{mag} in strong lensing, aiding in distinguishing the images from those associated with Schwarzschild BHs.

(e) The Einstein rings. For the supermassive BHs $M87^*$ and $SgrA^*$, we present the outermost Einstein rings θ_1^E for various cases: $\alpha = 0, 0.02, 0.04, 0.06, 0.08, 0.1$ for $\beta = 0.02$, and $\beta = 0, 0.01, 0.03, 0.05, 0.07, 0.0.9$ for $\alpha = 0.07$. These results are illustrated in Fig. 7. The radius of the outermost Einstein ring θ_1^E decreases with increasing values of the decoupling modified BH parameter α, for fixed β, and conversely decreases with increasing values of the decoupling modified BH parameter β, for fixed α. Our results indicate that the outermost Einstein ring θ_1^E for the decoupling modified BH is significantly smaller than that for a Schwarzschild BH. Consequently, a notable effect of the decoupling modified BH is evident on the strong lensing observable, the angular position of the images θ_∞, enabling the distinction of these images from those associated with other Schwarzschild BHs.

(f) Relativistic time delay. We have estimated the time-delays $\Delta T_{2,1}$ between the first and second-order relativistic images for various supermassive BHs located near the centers of galaxies, considering decoupling modified BHs with parameters $\alpha = 0.4$ and $\beta = 0.3$, as well as a Schwarzschild BH with $\alpha = 0$ (see Table 3). It is observed that the time delays for the decoupling modified BH with $\alpha = 0.4$ and $\beta = 0.3$ (e.g., NGC 7768, 1507.51 minutes) are shorter than those for the Schwarzschild BH (3582.72 minutes). Furthermore, the deviation of the time delays for a decoupling modified BH, denoted as $\delta\Delta T_{2,1}$, from those for the Schwarzschild BH is illustrated in Fig. 8 for the parameters α and β for the supermassive BHs M87* and Sgr A*. From Fig. 8, it is observed that the deviation $\delta\Delta T_{2,1}$ increases with the increasing value of the parameter β for a specific fixed value of the parameter α. Given that the time delays for the decoupling modified BH with $\alpha = 0.4$ and $\beta = 0.3$ are shorter than those for the Schwarzschild BH, there is a significant effect of the decoupling modified BH parameters on the strong lensing observable time delays between the first and second relativistic images, $\delta\Delta T_{2,1}$, enabling the distinction of these images from those associated with Schwarzschild BHs. This suggests that separating the first and second relativistic images and analyzing their time delay could provide a promising method to distinguish a decoupling modified BH from a Schwarzschild BH. Thus the findings in our observation, it is suggested that the decoupling modified BH is quantitatively distinguished from other astrophysical BHs like Schwarzschild BHs.Therefore, future observations aimed at discerning decoupling modified BHs from other astrophysical BHs, such as Schwarzschild BHs, hold significant importance. These observations could provide invaluable insights into the unique characteristics and behaviors of decoupling modified BHs, further enriching our understanding of gravitational lensing phenomena and the fundamental nature of BHs in the universe.

5 Summary and conclusions

In this paper, we have studied the strong gravitational lensing phenomena by the decoupling of modified BH in the context of various supermassive BHs in the center of nearby galaxies. For this purpose, we apply the methodology introduced by Bozza [70], which can be used to distinguish between various types of astrophysical spherically symmetric BHs and also discuss their various astrophysical consequences via strong gravitational lensing. Firstly, we calculate the lensing coefficients $\bar{a}, \bar{b}, u_c/R_s$. Subsequently, utilizing these coefficients, we determine the strong deflection angle α_D and various observable quantities-θ_∞, S, r_{mag}, Einstein's ring and time delays for several supermassive BHs located at the centers of nearby galaxies.

We numerically evaluated the strong lensing observables quantities for the relativistic images for the three supermassive BHs $M87^*$, $SgrA^*$ and $NGC4649$ in the context of the decoupling of modified BHs.

It is obtained that for the case when $\beta = 0.02$ and $0.01 \leq \alpha \leq 0.05, \theta_\infty \in (17.88, 19.47)\,\mu as$ for $M87^*, \theta_\infty \in (23.81, 25.91\,\mu as$ for $SgrA*$, $\theta_\infty \in (13.25, 14.43)\,\mu as$ for NGC 4649; for the case where $\beta = 0.04$ and $0.01 \leq \alpha \leq 0.05$, $\theta_\infty \in (18.17, 19.512)\,\mu as$ for $M87^*$, $\theta_\infty \in (24.18, 25.971)\,\mu as$ for $SgrA*$, $\theta_\infty \in (13.46, 14.462)\,\mu as$ for NGC 4649; and the case where$\beta = 0.06$ and $0.01 \leq \alpha \leq 0.05$, $\theta_\infty \in (18.33, 19.54)\,\mu as$ for $M87^*$, $\theta_\infty \in (24.39, 26.01)\,\mu as$ for $SgrA*$, $\theta_\infty \in (13.58, 14.482)\,\mu as$ for NGC 4649.

Another observable quantity, the angular separation $S \in (0.026, 0.034)\mu as$ for $M87^*$, $S \in (0.034, 0.045)\,\mu as$ for $SgrA^*$, $S \in (0.0193, 0.025)\,\mu as$ for NGC 4649 for the case when $\beta = 0.02$ and $0.01 \leq \alpha \leq 0.05$; $S \in (0.025, 0.032)\mu as$ for $M87^*$, $S \in (0.034, 0.042)\,\mu as$ for $SgrA^*$, $S \in (0.019, 0.0234)\,\mu as$ for NGC 4649 for the case when $\beta = 0.04$ and $0.01 \leq \alpha \leq 0.05$; and $S \in (0.0256, 0.0304)\mu as$ for $M87^*$, $S \in (0.034, 0.040431)\,\mu as$ for $SgrA^*$, $S \in (0.019, 0.023)\,\mu as$ for NGC 4649 for the case when$\beta = 0.06$ and $0.01 \leq \alpha \leq 0.05$. In other observable quantities, the relative magnification of the relativistic images r_{mag} is decreasing with the parameter α for the fixed value of $\beta(= 0.02, 0.04, 0.06)$; and is increasing with the parameter β for the fixed value of $\alpha(= 0.01, 0.02, 0.03, 0.04, 0.05)$;and for $0.01 \leq \alpha \leq 0.05$, $r_{mag} \in (6.42, 6.75)$, $r_{mag} \in (6.505, 6.769)$ and $r_{mag} \in (6.55, 6.78)$ order of magnitude respectively for the cases of $\beta = 0.02$, $\beta = 0.04$ and $\beta = 0.06$. By taking the supermassive BHs $SgrA^*$ and $M87^*$, the outermost Einstein ring θ_1^E with the different value of decoupling modified BH parameters α and β are depicted in Fig. 7. It has been observed that for the fixed value of the parameter, β the radius of the outermost Einstein ring θ_1^E decreases with the parameter α and also for the fixed value of the parameter α the radius of the outermost Einstein ring θ_1^E decreases with the parameter β. The angular radius θ_1^E of the outermost Einstein ring in the context of decoupling modified BH is smaller than the corresponding case of the standard Schwarzschild BH $\alpha = 0$. We have also obtained the time-delays $\Delta T_{2,1}$ between first and second-order relativistic images for various supermassive BHs in the context of standard Schwarzschild ($\alpha = 0$) and decoupling modified BH ($\alpha = 0.4$, $\beta = 0.3$) BH. It is observed that the time delay $\Delta T_{2,1}$ for the case of decoupling modified BH ($\alpha = 0.4$, $\beta = 0.3$) BH (e.g.$\sim$ 202.502 min for NGC 7457) significantly smaller than the case standard Schwarzschild ($\alpha = 0$) BH. The findings in our strong gravitational lensing observations suggest that decoupling modified BH is distinguishable from the other astrophysical BHs, such as standard Schwarzschild ($\alpha = 0$) BH.

Acknowledgements G. Mustafa is very thankful to Prof. Gao Xianlong from the Department of Physics, Zhejiang Normal University, for his kind support and help during this research. The author SKM is also thankful for continuous support and encouragement from the administration of University of Nizwa.

Data Availibility Statement No new data were generated or analyzed in support of this research. [Authors' comment: No observational data has been generated to this study. This work has already included a comprehensive analysis and the corresponding calculations.]

Code Availability Statement This manuscript has no associated code/software. [Authors' comment: We use the Mathematica and Python software for numerical computation and graphical analysis of this problem. No other code/software was generated or analyzed during the current study.]

Funded by SCOAP[3].

References

1. R. Ruffini, J.A. Wheeler, Introducing the black hole. Phys. Today **24**(1), 30–41 (1971)
2. V. Frolov, I. Novikov, *Black Hole Physics: Basic Concepts and New Developments*, vol. 96 (Springer Science & Business Media, Berlin, 2012)
3. S.W. Hawking, Black hole explosions? Nature **248**(5443), 30–31 (1974)
4. S.W. Hawking, BHs and thermodynamics. Phys. Rev. D **13**(2), 191 (1976)
5. R. Perna, M. Chruslinska, A. Corsi, K. Belczynski, Binary black hole mergers within the LIGO horizon: statistical properties and prospects for detecting electromagnetic counterparts. Mon. Not. Roy. Astron. Soc. **477**(3), 4228–4240 (2018)
6. I. Cholis, On the gravitational wave background from black hole binaries after the first LIGO detections. J. Cosmol. Astropart. Phys. **2017**(06), 037 (2017)
7. B. Zackay, L. Dai, T. Venumadhav, J. Roulet, M. Zaldarriaga, Detecting gravitational waves with disparate detector responses: two new binary black hole mergers. Phys. Rev. D **104**(6), 063030 (2021)
8. B. Abbott, R. Abbott, T. Abbott, S. Abraham, F. Acernese, K. Ackley, C. Adams, R. Adhikari, V. Adya, C. Affeldt et al., GWTC-1: a gravitational-wave transient catalog of compact binary mergers observed by LIGO and VIRGO during the first and second observing runs. Phys. Rev. X **9**(3), 031040 (2019)
9. A. Królak, P. Verma, Recent observations of gravitational waves by LIGO and VIRGO detectors. Universe **7**(5), 137 (2021)
10. C. Liu, L. Shao, J. Zhao, Y. Gao, Multiband observation of LIGO/VIRGO binary black hole mergers in the gravitational-wave

transient catalog GWTC-1. Mon. Not. Roy. Astron. Soc. **496**(1), 182–196 (2020)
11. M. Dominik, E. Berti, R. O'Shaughnessy, I. Mandel, K. Belczynski, C. Fryer, D.E. Holz, T. Bulik, F. Pannarale, Double compact objects. iii. Gravitational-wave detection rates. Astrophys. J. **806**(2), 263 (2015)
12. H.T. Collaboration, EHT sees black hole shadow. High-Resolut. Imaging **3** (2019)
13. J. Ovalle, Searching exact solutions for compact stars in braneworld: a conjecture. Mod. Phys. Lett. A **23**(38), 3247–3263 (2008)
14. J. Ovalle, Braneworld stars: anisotropy minimally projected onto the brane, in *Gravitation and Astrophysics*. (World Scientific, Singapore, 2010), pp.173–182
15. J. Ovalle, Decoupling gravitational sources in general relativity: the extended case. Phys. Lett. B **788**, 213–218 (2019)
16. J. Ovalle, F. Linares, Tolman iv solution in the Randall–Sundrum braneworld. Phys. Rev. D **88**(10), 104026 (2013)
17. J. Ovalle, F. Linares, A. Pasqua, A. Sotomayor, The role of exterior Weyl fluids on compact stellar structures in Randall–Sundrum gravity. Class. Quantum Gravity **30**(17), 175019 (2013)
18. J. Ovalle, L.A. Gergely, R. Casadio, Brane-world stars with a solid crust and vacuum exterior. Class. Quantum Gravity **32**(4), 045015 (2015)
19. R. Casadio, J. Ovalle, R. Da Rocha, Classical tests of general relativity: brane-world sun from minimal geometric deformation. Europhys. Lett. **110**(4), 40003 (2015)
20. J. Ovalle, Decoupling gravitational sources in general relativity: from perfect to anisotropic fluids. Phys. Rev. D **95**(10), 104019 (2017)
21. J. Ovalle, R. Casadio, R. Da Rocha, A. Sotomayor, Anisotropic solutions by gravitational decoupling. Eur. Phys. J. C **78**, 1–11 (2018)
22. F.X.L. Cedeño, E. Contreras, Gravitational decoupling in cosmology. Phys. Dark Univ. **28**, 100543 (2020)
23. E. Contreras, Gravitational decoupling in 2+1 dimensional spacetimes with cosmological term. Class. Quantum Gravity **36**(9), 095004 (2019)
24. E. Contreras, P. Bargueño, Extended gravitational decoupling in 2+1 dimensional space-times. Class. Quantum Gravity **36**(21), 215009 (2019)
25. S. Maurya, A. Pradhan, F. Tello-Ortiz, A. Banerjee, R. Nag, Minimally deformed anisotropic stars by gravitational decoupling in Einstein–Gauss–Bonnet gravity. Eur. Phys. J. C **81**, 1–19 (2021)
26. S. Maurya, K.N. Singh, M. Govender, S. Hansraj, Gravitationally decoupled strange star model beyond the standard maximum mass limit in Einstein–Gauss–Bonnet gravity. Astrophys. J. **925**(2), 208 (2022)
27. S. Maurya, K.N. Singh, M. Govender, S. Ray, Complexity-free anisotropic solution of buchdahl's model and energy exchange between relativistic fluids by extended gravitational decoupling. Fortschritte der Physik 2300023 (2023)
28. S.K. Maurya, K.N. Singh, M. Govender, G. Mustafa, S. Ray, The effect of gravitational decoupling on constraining the mass and radius for the secondary component of gw190814 and other self-bound strange stars in f (q) gravity theory. Astrophys. J. Suppl. Ser. **269**(2), 35 (2023)
29. S. Maurya, G. Mustafa, M. Govender, K.N. Singh, Exploring physical properties of minimally deformed strange star model and constraints on maximum mass limit in f (q) gravity. J. Cosmol. Astropart. Phys. **2022**(10), 003 (2022)
30. J. Ovalle, R. Casadio, E. Contreras, A. Sotomayor, Hairy BHs by gravitational decoupling. Phys. Dark Univ. **31**, 100744 (2021)
31. N. Kaiser, G. Squires, Mapping the dark matter with weak gravitational lensing. Astrophys. J. **404**, 441–450 (1993). https://doi.org/10.1086/172297
32. Y. Wang, A. Stebbins, E.L. Turner, Gravitational lensing of gravitational waves from merging neutron star binaries. Phys. Rev. Lett. **77**(14), 2875 (1996)
33. L.C.B. Crispino, D. Kennefick, 100 years of the first experimental test of General Relativity. Nat. Phys. **15**, 416 (2019). https://doi.org/10.1038/s41567-019-0519-3
34. S. Frittelli, T.P. Kling, E.T. Newman, Space-time perspective of Schwarzschild lensing. Phys. Rev. D **61**, 064021 (2000). https://doi.org/10.1103/PhysRevD.61.064021. arXiv:gr-qc/0001037
35. K.S. Virbhadra, D. Narasimha, S.M. Chitre, Role of the scalar field in gravitational lensing. Astron. Astrophys. **337**, 1–8 (1998). arXiv:astro-ph/9801174
36. K.S. Virbhadra, G.F.R. Ellis, Schwarzschild black hole lensing. Phys. Rev. D **62**, 084003 (2000). https://doi.org/10.1103/PhysRevD.62.084003. arXiv:astro-ph/9904193
37. V. Perlick, On the exact gravitational lens equation in spherically symmetric and static space-times. Phys. Rev. D **69**, 064017 (2004). https://doi.org/10.1103/PhysRevD.69.064017. arXiv:gr-qc/0307072
38. G.Z. Babar, F. Atamurotov, A.Z. Babar, Gravitational lensing in 4-D Einstein–Gauss–Bonnet gravity in the presence of plasma. Phys. Dark Univ. **32**, 100798 (2021). https://doi.org/10.1016/j.dark.2021.100798. arXiv:2103.00316
39. F. Atamurotov, A. Abdujabbarov, W.-B. Han, Effect of plasma on gravitational lensing by a Schwarzschild black hole immersed in perfect fluid dark matter. Phys. Rev. D **104**(8), 084015 (2021). https://doi.org/10.1103/PhysRevD.104.084015
40. F. Atamurotov, U. Papnoi, K. Jusufi, Shadow and deflection angle of charged rotating black hole surrounded by perfect fluid dark matter. Class. Quantum Gravity **39**(2), 025014 (2022). https://doi.org/10.1088/1361-6382/ac3e76. arXiv:2104.14898
41. F. Atamurotov, S.G. Ghosh, Gravitational weak lensing by a naked singularity in plasma. Eur. Phys. J. Plus **137**(6), 662 (2022). https://doi.org/10.1140/epjp/s13360-022-02885-3
42. G. Mustafa, F. Atamurotov, I. Hussain, S. Shaymatov, A. Övgün, Shadows and gravitational weak lensing by the Schwarzschild black hole in the string cloud background with quintessential field*. Chin. Phys. C **46**(12), 125107 (2022). https://doi.org/10.1088/1674-1137/ac917f. arXiv:2207.07608
43. F. Atamurotov, I. Hussain, G. Mustafa, A. Övgün, Weak deflection angle and shadow cast by the charged-Kiselev black hole with cloud of strings in plasma*. Chin. Phys. C **47**(2), 025102 (2023). https://doi.org/10.1088/1674-1137/ac9fbb
44. F. Atamurotov, M. Jamil, K. Jusufi, Quantum effects on the black hole shadow and deflection angle in the presence of plasma*. Chin. Phys. C **47**(3), 035106 (2023). https://doi.org/10.1088/1674-1137/acaef7. arXiv:2212.12949
45. A. Ditta, X. Tiecheng, S. Mumtaz, F. Atamurotov, G. Mustafa, A. Abdujabbarov, Testing metric-affine gravity using particle dynamics and photon motion. Phys. Dark Univ. **41**, 101248 (2023). https://doi.org/10.1016/j.dark.2023.101248. arXiv:2303.05438
46. N.U. Molla, H. Chaudhary, D. Arora, F. Atamurotov, U. Debnath, G. Mustafa, Strong gravitational lensing by Sgr A* and M87* BHs embedded in dark matter halo exhibiting string cloud and quintessential field. (10) (2023). arXiv:2310.14234
47. F. Atamurotov, K. Jusufi, M. Jamil, A. Abdujabbarov, M. Azreg-Aïnou, Axion-plasmon or magnetized plasma effect on an observable shadow and gravitational lensing of a Schwarzschild black hole. Phys. Rev. D **104**(6), 064053 (2021). https://doi.org/10.1103/PhysRevD.104.064053. arXiv:2109.08150
48. G.Z. Babar, F. Atamurotov, S. Ul Islam, S.G. Ghosh, Particle acceleration around rotating Einstein–Born–Infeld black hole and plasma effect on gravitational lensing. Phys. Rev. D **103**(8), 084057 (2021). https://doi.org/10.1103/PhysRevD.103.084057. arXiv:2104.00714

49. A. Abdujabbarov, B. Ahmedov, N. Dadhich, F. Atamurotov, Optical properties of a braneworld black hole: gravitational lensing and retrolensing. Phys. Rev. D **96**(8), 084017 (2017). https://doi.org/10.1103/PhysRevD.96.084017
50. R. Shaikh, P. Banerjee, S. Paul, T. Sarkar, Analytical approach to strong gravitational lensing from ultracompact objects. Phys. Rev. D **99**(10), 104040 (2019)
51. R. Kumar, S.G. Ghosh, A. Wang, Shadow cast and deflection of light by charged rotating regular BHs. Phys. Rev. D **100**(12), 124024 (2019)
52. R. Kumar, B.P. Singh, S.G. Ghosh, Shadow and deflection angle of rotating black hole in asymptotically safe gravity. Ann. Phys. **420**, 168252 (2020)
53. R. Kumar, S.G. Ghosh, A. Wang, Gravitational deflection of light and shadow cast by rotating Kalb–Ramond BHs. Phys. Rev. D **101**(10), 104001 (2020)
54. S.U. Islam, R. Kumar, S.G. Ghosh, Gravitational lensing by BHs in the 4*D* Einstein–Gauss–Bonnet gravity. JCAP **09**, 030 (2020)
55. J. Kumar, S.U. Islam, S.G. Ghosh, Investigating strong gravitational lensing effects by supermassive BHs with Horndeski gravity. Eur. Phys. J. C **82**(5), 443 (2022)
56. S.U. Islam, S.G. Ghosh, Strong field gravitational lensing by hairy Kerr BHs. Phys. Rev. D **103**(12), 124052 (2021). https://doi.org/10.1103/PhysRevD.103.124052. arXiv:2102.08289
57. S.G. Ghosh, R. Kumar, S.U. Islam, Parameters estimation and strong gravitational lensing of nonsingular Kerr–Sen BHs. JCAP **03**, 056 (2021)
58. J. Kumar, S.U. Islam, S.G. Ghosh, Testing strong gravitational lensing effects of supermassive compact objects with regular spacetimes. Astrophys. J. **938**(2), 104 (2022)
59. R. Kumar, S.U. Islam, S.G. Ghosh, Gravitational lensing by charged black hole in regularized 4*D* Einstein–Gauss–Bonnet gravity. Eur. Phys. J. C **80**(12), 1128 (2020)
60. C. Avestruz, N. Li, H. Zhu, M. Lightman, T.E. Collett, W. Luo, Automated lensing learner: automated strong lensing identification with a computer vision technique. Astrophys. J. **877**(1), 58 (2019)
61. A. Zitrin, T. Broadhurst, Strong-lensing analysis of the powerful lensing cluster MACS J2135. 2–0102 (z= 0.33). Astrophys. J. **833**(1), 25 (2016)
62. A. Övgün, I. Sakallı, Testing generalized Einstein–Cartan–Kibble–Sciama gravity using weak deflection angle and shadow cast. Class. Quantum Gravity **37**(22), 225003 (2020)
63. A. Övgün, I. Sakallı, J. Saavedra, Shadow cast and deflection angle of Kerr–Newman–Kasuya spacetime. J. Cosmol. Astropart. Phys. **10**, 041 (2018)
64. A. Övgün, I. Sakallı, J. Saavedra, Effect of null aether field on weak deflection angle of black holes. Chin. Phys. C **44**(12), 125105 (2020)
65. N.U. Molla, U. Debnath, Gravitational lensing of acoustic charged BHs. Astrophys. J. **947**(1), 14 (2023). https://doi.org/10.3847/1538-4357/acb6f2
66. N.U. Molla, U. Debnath, Shadows and strong gravitational lensing by Van der Waals black hole in homogeneous plasma. Ann. Phys. **453**, 169304 (2023). https://doi.org/10.1016/j.aop.2023.169304. arXiv:2212.02104
67. N.U. Molla, U. Debnath, Gravitational lensing for power-Maxwell charged quintessence black hole in Rastall gravity. Int. J. Geom. Methods Mod. Phys. **19**(12), 2250183 (2022)
68. N.U. Molla, U. Debnath, Strong gravitational lensing by Kerr–Newman-NUT-Quintessence black hole. Int. J. Mod. Phys. A **36**(27), 2150210 (2021). https://doi.org/10.1142/S0217751X21502109
69. J.L. Synge, The escape of photons from gravitationally intense stars. Mon. Not. Roy. Astron. Soc. **131**(3), 463–466 (1966). https://doi.org/10.1093/mnras/131.3.463
70. V. Bozza, Gravitational lensing in the strong field limit. Phys. Rev. D **66**, 103001 (2002)
71. R. Avalos, P. Bargueño, E. Contreras, A static and spherically symmetric hairy black hole in the framework of the gravitational decoupling. Fortschr. Phys. **71**, 2200171 (2023)
72. J. Ovalle, R. Casadio, R.D. Rocha, A. Sotomayor, Z. Stuchlík, BHs by gravitational decoupling. Eur. Phys. J. C **78**, 1–11 (2018)
73. L. Balart, E.C. Vagenas, Regular BHs with a nonlinear electrodynamics source. Phys. Rev. D **90**(12), 124045 (2014)
74. K.S. Virbhadra, G.F.R. Ellis, Gravitational lensing by naked singularities. Phys. Rev. D **65**, 103004 (2002)
75. N. Tsukamoto, Strong deflection limit analysis and gravitational lensing of an Ellis wormhole. Phys. Rev. D **94**(12), 124001 (2016). https://doi.org/10.1103/PhysRevD.94.124001. arXiv:1607.07022
76. S.V. Iyer, A.O. Petters, Light's bending angle due to BHs: from the photon sphere to infinity. Gen. Relat. Gravit. **39**, 1563–1582 (2007). https://doi.org/10.1007/s10714-007-0481-8. arXiv:gr-qc/0611086
77. N. Tsukamoto, Deflection angle in the strong deflection limit in a general asymptotically flat, static, spherically symmetric spacetime. Phys. Rev. D **95**(6), 064035 (2017). https://doi.org/10.1103/PhysRevD.95.064035. arXiv:1612.08251
78. N. Tsukamoto, Gravitational lensing by using the 0th order of affine perturbation series of the deflection angle of a ray near a photon sphere. Eur. Phys. J. C **83**(4), 284 (2023). https://doi.org/10.1140/epjc/s10052-023-11419-9. arXiv:2211.04239
79. N. Tsukamoto, Affine perturbation series of the deflection angle of a ray near the photon sphere of a Reissner–Nordström black hole. Phys. Rev. D **106**(8), 084025 (2022). https://doi.org/10.1103/PhysRevD.106.084025. arXiv:2208.10197
80. V. Bozza, S. Capozziello, G. Iovane, G. Scarpetta, Strong field limit of black hole gravitational lensing. Gen. Relat. Gravit. **33**, 1535–1548 (2001)
81. K. Akiyama et al., First M87 event horizon telescope results. I. The shadow of the supermassive black hole. Astrophys. J. Lett. **875**, L1 (2019). https://doi.org/10.3847/2041-8213/ab0ec7. arXiv:1906.11238
82. S. Gillessen, P. Plewa, F. Eisenhauer, R. Sari, I. Waisberg, M. Habibi, O. Pfuhl, E. George, J. Dexter, S. von Fellenberg et al., An update on monitoring stellar orbits in the galactic center. Astrophys. J. **837**(1), 30 (2017)
83. J. Kormendy, L.C. Ho, Coevolution (or not) of supermassive BHs and host galaxies. Ann. Rev. Astron. Astrophys. **51**, 511–653 (2013)
84. A. Einstein, Lens-like action of a star by the deviation of light in the gravitational field. Science **84**, 506–507 (1936)
85. S. Liebes, Gravitational lenses. Phys. Rev. **133**, B835–B844 (1964)
86. Y. Mellier, Probing the universe with weak lensing. Ann. Rev. Astron. Astrophys. **37**, 127–189 (1999)
87. M. Bartelmann, P. Schneider, Weak gravitational lensing. Phys. Rep. **340**, 291–472 (2001)
88. F. Schmidt, Weak lensing probes of modified gravity. Phys. Rev. D **78**, 043002 (2008)
89. J. Guzik, B. Jain, M. Takada, Tests of gravity from imaging and spectroscopic surveys. Phys. Rev. D **81**, 023503 (2010)
90. V. Bozza, L. Mancini, Time delay in black hole gravitational lensing as a distance estimator. Gen. Relat. Gravit. **36**, 435–450 (2004)
91. N.U. Molla, H. Chaudhary, G. Mustafa, U. Debnath, S.K. Maurya, Strong gravitational lensing, quasi-periodic oscillations and constraints from EHT observations for quantum-improved charged black hole. Eur. Phys. J. C **84**(4), 390 (2024)
92. E.L.B. Junior, F.S.N. Lobo, M.E. Rodrigues, H.A. Vieira, Gravitational lens effect of a holonomy corrected Schwarzschild black hole. Phys. Rev. D **109**(2), 2 (2024)

93. J. Kumar, S. Ul Islam, S.G. Ghosh, Strong gravitational lensing by loop quantum gravity motivated rotating BHs and EHT observations. Eur. Phys. J. C **83**(11), 1014 (2023)
94. T.C. Frost, Gravitational lensing of massive particles in the charged NUT spacetime. Phys. Rev. D **108**(12), 124019 (2023)
95. S.K. Jha, A. Rahaman, Strong gravitational lensing in hairy Schwarzschild background. Eur. Phys. J. Plus **138**(1), 86 (2023)
96. S. Ul Islam, S.G. Ghosh, S.D. Maharaj, Strong gravitational lensing by Bardeen BHs in 4D EGB gravity: constraints from supermassive BHs. Chin. J. Phys. **89**, 1710–1724 (2024)
97. S.G. Ghosh, S. Ul Islam, Gravitational lensing by rotating Simpson–Visser BHs. MG16, pp. 3812–3826
98. N.U. Molla, S.G. Ghosh, U. Debnath, Testing gravitational lensing effects by supermassive massive BHs with superstring theory metric: astrophysical implications and EHT constraints. Phys. Dark Univ. **44**, 101495 (2024)
99. A. Vachher, D. Baboolal, S.G. Ghosh, Probing dark matter via strong gravitational lensing by black holes. Phys. Dark Univ. **44**, 101493 (2024)